Program Digest, 2019 IEEE International Ultrasonics Symposium (IUS)
Glasgow, Scotland, October 6-9, 2019

# Motion Compensation for High-Frame-Rate Contrast-Enhanced Echocardiography Using Diverging Waves: Image Registration Versus Correlation-Based Method

Luzhen Nie[1], David M. J. Cowell[1], Thomas M. Carpenter[1], James R. McLaughlan[1,2], Arzu A. Çubukçu[3], and Steven Freear[1]
[1]Ultrasound Group, School of Electronic and Electrical Engineering, University of Leeds, Leeds LS2 9JT, U.K.
[2] Leeds Institute of Cancer and Pathology, University of Leeds, Leeds LS9 7TF, U.K.
[3] East Cheshire NHS Trust, Macclesfield, SK10 3BL, U.K.
E-mail: elln@leeds.ac.uk and s.freear@leeds.ac.uk

***Abstract*—By using diverging ultrasound waves, a B-mode image can be reconstructed from a single transmission with parallel beamforming. For echocardiography, this approach can provide a frame rate up to 5 kHz, which is two orders of magnitude faster than the most clinical scanners. However, image degradation arising from the lack of transmit focusing when using diverging waves, could not be alleviated by coherent compounding due to the effect of cardiac motion. The motion effects on high-frame-rate contrast-enhanced echocardiography (HFR CEE) when combining diverging waves and microbubble contrast agents were demonstrated in recent studies, with a two-stage correlation-based method and an image registration-based method proposed to enable coherent compounding. The current study compared these two methods for motion compensation in HFR CEE both *in vitro* and *in vivo*. For *in vitro* experiments with a rotating disk phantom, the correlation-based method improved the contrast ratio and contrast-to-noise-ratio by 5 dB and 3 dB, respectively. For the *in vivo* measurement, the correlation-based method provided a 6-dB improvement in contrast-to-tissue ratio.**

## I. Introduction

The capability of exciting and sampling each individual element of an array transducer has spawned a branch of high-frame-rate (HFR) ultrasound imaging using plane/diverging waves (DWs) [1]. HFR ultrasound technology opens new vistas for the development of new methods for vector flow mapping [2], tissue elasticity mapping [3] and functional brain imaging [4]. The advent of HFR contrast-enhanced echocardiography (CEE) using DWs could improve the ways to assess cardiac function, by providing a higher contrast-to-tissue ratio (CTR) [5] and depicting the intracardiac blood flow with a high temporal resolution [6]. It was recently demonstrated that coherent compounding is ineffective due to motion artefacts, and there may be necessity of developing motion compensation methods for HFR CEE [7], [8]. A correlation-based [7] and an image registration-based [8] schemes have been proposed to compensate for incoherence between angled transmissions. The current study aimed to compare their relative performance in terms of contrast ratio (CR) and contrast-to-noise ratio (CNR) *in vitro*, and contrast-to-tissue ratio (CTR) *in vivo*.

## II. Methods

### A. Imaging Setup

The 4-cycle 2.78 MHz ultrasound pulses were designed to emanate DWs with the full aperture at each steering angle. The sector angle was set to 90° and unchanged during beam steering for compounding. The steering angles were ($-10°$, $-8°$, $-6°$, $-4°$, $4°$, $6°$, $8°$, $10°$). The Ultrasound Array Research Platform (UARP) II equipped with a Verasonics P4-2v transducer was used for *in vitro* and *in vivo* measurements with a mechanical index (MI) of 0.12 and a pulse repetition frequency (PRF) of 4 kHz. The *in vitro* rotating disk phantom had a diameter of 10 cm with 4 equidistant 12.8-mm anechoic cysts, and it was rotated at $4\pi$ rad/s. Amplitude modulation (AM) was incorporated at each steering angle for the *in vivo* investigation with a 1-mL bolus of SonoVue microbubbles.

### B. Correlation-Based Technique

A two-stage method was developed to find the correlation and subpixel displacement between angled low-resolution images (LRIs) in the polar coordinate system. The first stage used rigid block matching between all consecutive frames to find the averaged global estimation. The second stage used an iterative scheme to improve the resolution and accuracy of the motion estimation by recursively decreasing the kernel size and deforming the kernel based on the results from the previous iteration. Two iterations was used in the second stage. The resultant motion estimation for each pixel was then obtained by linearly interpolating the motion estimation results from the last iteration of motion estimation in the second stage. Based on these estimated displacements, motion compensation was then performed by realigning image pixels of all LRIs prior to coherent compounding. All LRIs with motion were registered to the first LRI within the set used for coherent

978-1-7281-4595-2/19/$31.00 ©2019 IEEE 

TABLE I
PARAMETERS FOR BEAMFORMING AND MOTION COMPENSATION

| Parameter | Value |
|---|---|
| Pixel size (radial) | 38.5 $\mu$m |
| Pixel size (angular) | 0.0625° |
| Kernel size (1st stage) | 152x84 (radial and angular lines) |
| Kernel size (2nd stage) | 76x42; 38x21 |
| Kernel overlap | 50% |

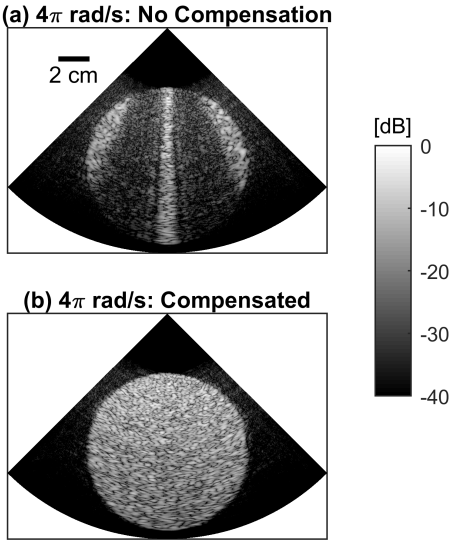


Fig. 1. B-mode compound images of the simulated rotating disk (a) without and (b) with motion compensation in the polar coordinate system.

compounding in this study. All specific parameters are given in Table I. More details about this method can be found in [7].

The rationale of using the polar coordinate system instead of the Cartesian coordinate system was first explained using a Field II simulated disk phantom with a diameter of 10 cm. With a rotation speed of $4\pi$ rad/s as used for *in vitro* measurements, the associated B-mode images with and without motion compensation are shown in Fig. 1 and Fig. 2. Fig. 1 shows the results when the polar coordinate system was used, and Fig. 2 shows the results when motion estimation was performed in the Cartesian coordinate system. The most accurate motion estimation occurs along the direction of beam propagation. In Fig. 2, the interpretation of the disk is difficult due to the dark artefacts, where motion tracking does not follow the propagation direction of the diverging wave. The window size [(lateral distance x depth)] was varied between (3 mm x 2.95 mm), (6 mm x 5.9 mm), and (12 mm x 11.8 mm). For all used window sizes, the imaging artefacts were not avoided. For Fig. 2, the window size of (6 mm x 5.9 mm) was used.

### C. Image Registration-Based Technique

Image registration is prevalent in fusing different imaging modalities (e.g. MRI and ultrasound). It is a process of aligning images so that corresponding features can be related. For cardiac imaging, tissue deformation needs to be

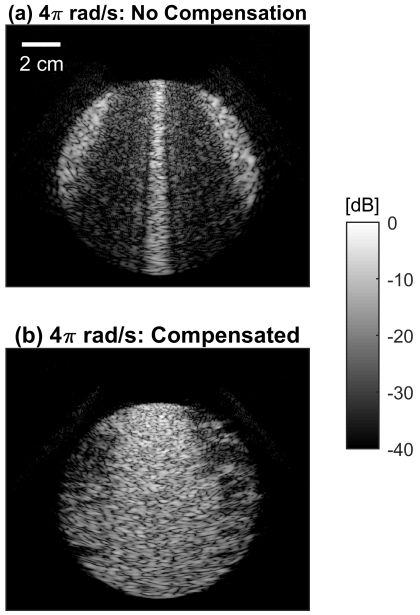


Fig. 2. B-mode compound images of the simulated rotating disk (a) without and (b) with motion compensation in the Cartesian coordinate system.

accommodated, requiring nonrigid registration. Each nonrigid registration technique can be described with three components: a transformation matrix between the source and target images, the similarity index between these two images, and an optimisation function that optimises the similarity index and tunes the transformation matrix accordingly. In [9], a combined transformation matrix $T$ consisting of a global ($T_{\mathrm{global}}$) and a local ($T_{\mathrm{local}}$) transformation is formed

$$T(x, y, z) = T_{\mathrm{global}}(x, y, z) + T_{\mathrm{local}}(x, y, z). \quad (1)$$

For global motion, an affine transformation which can describe scaling and shearing is modelled. A free-form deformation based on B-splines is used to model nonrigid local motion by manipulating the underlying mesh of control points. Increasing resolution of the mesh control points can be achieved by refining the control point mesh, having decreased control point spacing at the current level. The nonrigid local deformation is optimised by a smooth transformation and the measurement of image similarity. To constrain the B-spline-based transformation to be smooth, a penalty term $C_{\mathrm{smooth}}$ is introduced. The measurement of image similarity $C_{\mathrm{similarity}}$ can be performed based on the normalized mutual information which relies on the concept of information theory, or the squared sum of intensity differences. A cost function is written to find the optimal transformation as follows:

$$C = -C_{\mathrm{similarity}}(I(t_0), T(I(t))) + \lambda_{\mathrm{w}} C_{\mathrm{smooth}}(T), \quad (2)$$

where $I(t_0)$ is the image intensity at $t_0$, and $I(t)$ is the image intensity at $t$. Here, the weighting parameter $\lambda_{\mathrm{w}}$ regulates the tradeoff between the image alignment and transformation smoothness. It is shown that the choice of this parameter is not

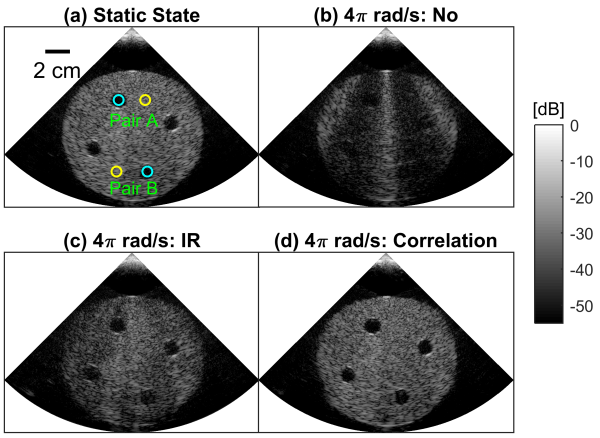


Fig. 3. Compound images of the *in vitro* disk in the (a) static state, the rotating state (b) without motion compensation, and the rotating state compensated with (c) the image registration technique, and (d) the correlation-based method. IR: image registration.

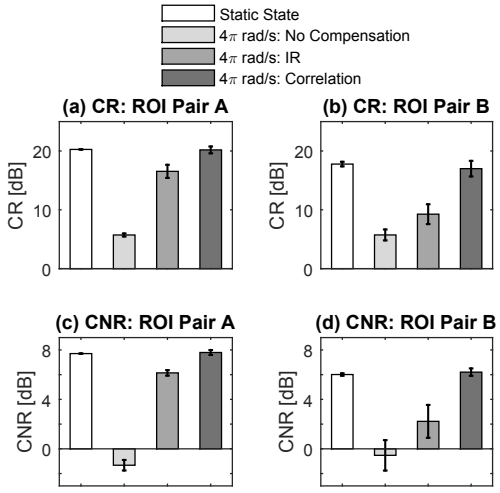


Fig. 4. CRs and CNRs for two pairs of ROIs as shown in Fig. 3(a). The mean values and standard deviations are based on 4 measurements. IR: image registration.

crucial and a range between 0.001 and 0.1 is acceptable for ultrasound imaging applications [10]. The optimisation proceeds in two stages. In the first stage, the affine transformation parameters are optimised by using an iterative multiresolution method, coping with the global motion. In the subsequent second stage, the parameters for nonrigid transformation are optimised in line with the cost function given in Eq. 2. The optimisation stops in practice when the change of the cost function is smaller than a predefined value.

In this study, the image registration model proposed in [8], [9] was applied to the LRIs in the polar grid before coherent summation of low-resolution B-mode and AM contrast-mode images. During image registration, the default parameters for 2-D images were used. The first LRI within the set was used as the reference for registration.

## III. Results

For *in vitro* measurements with the rotating disk phantom, two pairs of ROIs were delineated as shown in Fig. 3(a), with which the CR and CNR were calculated. Using the image registration technique for motion correction, coherent compounding was partially improved, with the dark region reduced as shown in Fig. 3(c). With the correlation-based method, the artefacts from the original B-mode compound image (Fig. 3b) were removed without any smearing of the image as shown in Fig. 3(d). The CRs and CNRs were improved with the integration of both motion compensation strategies as shown in Fig. 4. Whereas in all cases, the improvement is more manifest when using the correlation-based method. This is particularly true for ROI pair B placed at a deeper location. The correlation-based method was found to improve the CR and CNR by 5 dB and 3 dB (mean values for ROI pairs A and B), respectively, when compared with the image registration model. The lower level of SNR for ROI pair B is expected, during image registration the operation of optimisation to minimise the cost function will take noise into account, deteriorating its performance for motion compensation.

Fig. 5(a) shows the ROIs for the calculation of CTR *in vivo*. Without motion compensation, dark imaging artefacts were found in Fig. 5(a) and Fig. 5(d). The use of the image registration model reduced the dark imaging artefacts (Fig. 5b and Fig. 5e). The correlation-based method further reduced the imaging artefacts as shown in Fig. 5(c), and a 6-dB improvement of CTR (4.7 dB vs. 10.8 dB) was obtained when comparing Fig. 5(e) and Fig. 5(f).

## IV. Discussion

The motion estimation was performed with a static reference (the first LRI) when using the image registration technique. The selection of the reference frame is thus crucial and could disrupt motion correction if the reference frame has a low SNR. To further elaborate, image registration between each pair of consecutive frames was further carried out, giving the motion field for each pair. Motion compensation was then performed by counter-shifting the LRIs based on the accumulated motion field calculated from each pair of consecutive frames. Fig. 6(a) shows the corresponding compound image of the *in vitro* rotating disk phantom with the same RF data used for Fig. 3. Instead, for Fig. 6(b) the motion fields from all pairs of consecutive frames were first averaged, and the average displacement was used for motion correction, as used in Section II-B. In Fig. 6, both images are presented with the first LRI as the registered state. It is visible that the geometrical border of the disk is still largely affected by the dark imaging artefacts when using these two adapted schemes based on image registration.

## V. Conclusion

The correlation-based method provided a 5-dB and 3-dB increase in CR and CNR, respectively, *in vitro*, with the improved visibility of borders of a rotating disk phantom.

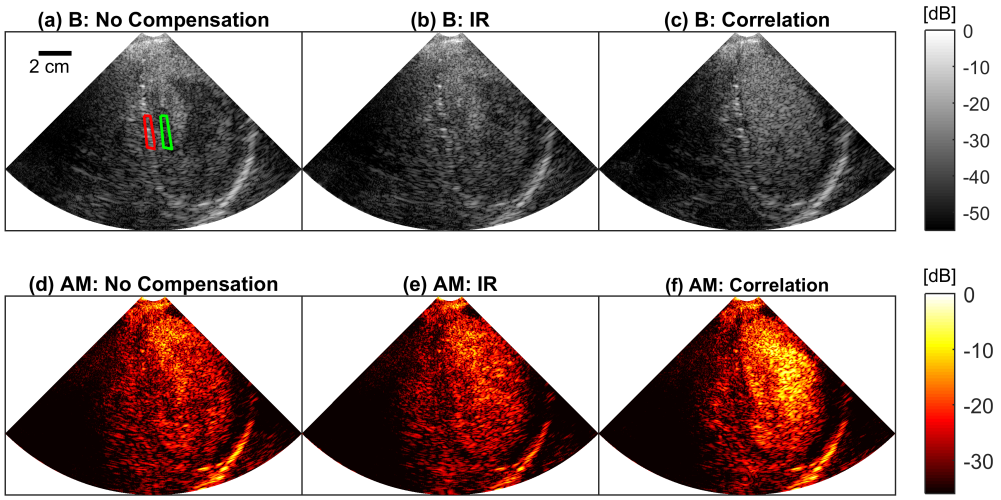


Fig. 5. Synchronized B-mode and contrast-mode compound images from the same AM pulse sequence consisting of 16 pulse transmissions. Image registration-based motion compensation was applied to (b) and (e), and the correlation-based method was used for (c) and (f). IR: image registration.

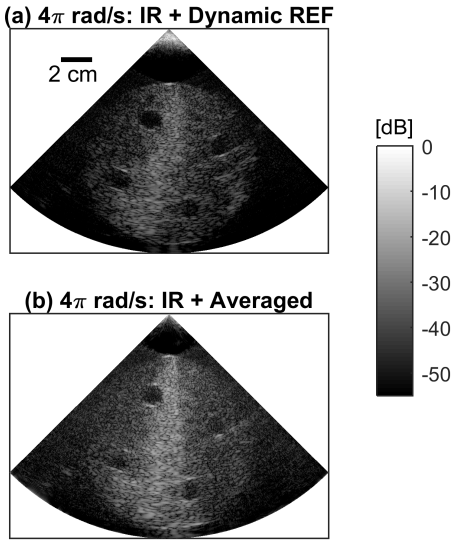


Fig. 6. The RF data used for Fig. 3 was reprocessed using image registration-based motion correction with (a) dynamic references and (b) the averaged motion filed. IR: image registration. REF: reference.

Compared against the image registration method, a 6-dB CTR improvement in contrast-enhanced imaging was also quantitatively demonstrated *in vivo*. Overall, the correlation-based method outperformed the image registration algorithm in preserving the efficacy of coherent compounding for HFR CEE using DWs.

## VI. Acknowledgement

This work was supported by the EPSRC under Grant EP/P023266/1 and EP/N034813/1. J. R. McLaughlan would like to acknowledge support from an EPSRC Innovation Fellowship EP/S001069/1.

## References

[1] E. Boni, A. C. H. Yu, S. Freear, J. A. Jensen, and P. Tortoli, "Ultrasound open platforms for next-generation imaging technique development," *IEEE Transactions on Ultrasonics, Ferroelectrics, and Frequency Control*, vol. 65, no. 7, pp. 1078–1092, July 2018.

[2] S. Ricci, A. Ramalli, L. Bassi, E. Boni, and P. Tortoli, "Real-time blood velocity vector measurement over a 2-d region," *IEEE Transactions on Ultrasonics, Ferroelectrics, and Frequency Control*, vol. 65, no. 2, pp. 201–209, Feb 2018.

[3] G. Montaldo, M. Tanter, J. Bercoff, N. Benech, and M. Fink, "Coherent plane-wave compounding for very high frame rate ultrasonography and transient elastography," *IEEE Transactions on Ultrasonics, Ferroelectrics, and Frequency Control*, vol. 56, no. 3, pp. 489–506, March 2009.

[4] E. Macé, G. Montaldo, I. Cohen, M. Baulac, M. Fink, and M. Tanter, "Functional ultrasound imaging of the brain," *Nature Methods*, vol. 8, no. 8, p. 662, 2011.

[5] M. Toulemonde, Y. Li, S. Lin, F. Cordonnier, M. Butler, W. C. Duncan, R. J. Eckersley, V. Sboros, and M. Tang, "High-frame-rate contrast echocardiography using diverging waves: Initial in vitro and in vivo evaluation," *IEEE Transactions on Ultrasonics, Ferroelectrics, and Frequency Control*, vol. 65, no. 12, pp. 2212–2221, Dec 2018.

[6] M. E. Toulemonde, R. Corbett, V. Papadopoulou, N. Chahal, Y. Li, C. H. Leow, D. O. Cosgrove, R. J. Eckersley, N. Duncan, R. Senior *et al.*, "High frame-rate contrast echocardiography: In-human demonstration," *JACC: Cardiovascular Imaging*, vol. 11, no. 6, pp. 923–924, 2018.

[7] L. Nie, D. M. J. Cowell, T. M. Carpenter, J. R. Mclaughlan, A. A. ubuku, and S. Freear, "High-frame-rate contrast-enhanced echocardiography using diverging waves: 2-d motion estimation and compensation," *IEEE Transactions on Ultrasonics, Ferroelectrics, and Frequency Control*, vol. 66, no. 2, pp. 359–371, Feb 2019.

[8] A. Stanziola, M. Toulemonde, Y. Li, V. Papadopoulou, R. Corbett, N. Duncan, R. J. Eckersley, and M. X. Tang, "Motion artifacts and correction in multipulse high-frame rate contrast-enhanced ultrasound," *IEEE Transactions on Ultrasonics, Ferroelectrics, and Frequency Control*, vol. 66, no. 2, pp. 417–420, Feb 2019.

[9] D. Rueckert, L. I. Sonoda, C. Hayes, D. L. G. Hill, M. O. Leach, and D. J. Hawkes, "Nonrigid registration using free-form deformations: application to breast mr images," *IEEE Transactions on Medical Imaging*, vol. 18, no. 8, pp. 712–721, Aug 1999.

[10] S. Harput, K. Christensen-Jeffries, J. Brown, Y. Li, K. J. Williams, A. H. Davies, R. J. Eckersley, C. Dunsby, and M. Tang, "Two-stage motion correction for super-resolution ultrasound imaging in human lower limb," *IEEE Transactions on Ultrasonics, Ferroelectrics, and Frequency Control*, vol. 65, no. 5, pp. 803–814, May 2018.